

Microtubular Protofilament Analysis Based on Molecular Level Tubulin Interaction

JongWon Kim^{1,2}, Ning Li², Ramana Pidaparti^{2,*} and Xianqiao Wang^{2,*}

Abstract: Nonlinear microstructure of the microtubules (MTs) plays an important role in their mechanical properties. Despite the extensive efforts into the development of continuum models for microtubules, a mesoscale finite element model that can link the molecular level information to the overall performance of microtubules is still missing. The aim of this study is to develop a molecular dynamics model (MDM), finite element model (FEM) and structural mechanics beam model (SMBM) for tubulins of protofilament (PF). In MDM, the backbone atoms of α -tubulin were fixed while the backbone atoms of β -tubulin were attached to a molecular dynamics (MD) atom through a virtual spring. In FEM, both α and β tubulins are modeled as spherical shells and adjacent tubulins are connected by linear springs. The spherical shells were framed as beams in SMBM. Corresponding parameters such as the elasticity of tubulin-tubulin interaction (TTI) and the stiffness of springs and beam are derived from MD simulation. Marginal differences in the force-deflection curve among the FEM, the MDM and SMBM indicate the good accuracy in describing the mechanical properties of microtubules. Simulation results show that the protofilament behaves non-linearly under tension and torsion but linearly under bending. Deformation pattern of a PF from the SMBM frame bending can be well captured by the classical Euler-Bernouli beam theory and the flexural rigidity derived from FEM is in good agreement with SMBM. These findings lend compelling credence in our developed models of PF to deepen our understanding of the underlying mechanism of statics and dynamics of MTs. In perspective our approach provides a tool for the analysis of MTs mechanical behavior under different conditions.

Keywords: Microtubule, protofilament, tubulin, molecular dynamics, finite element method, mechanical properties.

1 Introduction

Microtubules (MTs) are long filamentous hollow cylinders whose surfaces form lattice structures of $\alpha\beta$ -tubulin dimers. It is the largest type of cytoskeletal filaments and vital to

¹ Radiation Oncology, Medical College of Wisconsin, Wauwatosa, WI, 53327, USA.

² College of Engineering, University of Georgia, Athens, GA, 30605, USA.

* Corresponding Author: Ramana Pidaparti. Email: rmparti@uga.edu;

Xianqiao Wang . Email: xqwang@uga.edu.

many cellular functions, such as cell division, intracellular transport, cellular skeleton, etc. [Alberts (2017)] Due to their high rigidity, static microtubules play a very important role in maintaining cell morphology and adjusting subcellular structures [Valdman, Atzberger, Yu et al. (2012); Dogterom and Surrey (2013)]. In addition, their ability to undergo infrequent transitions between polymerization (growth) and de-polymerization (catastrophe or shortening) enables them to play a vital role in cell mitosis such as formation/positioning of the mitotic spindle and search/capture of mitotic chromosomes [Walczak, Cai and Khodjakov (2010)]. Moreover, inspired by the self-assembled structure of MTs, several designs of nanomaterial assemblies are proposed for multiple applications in sensing, medicine and etc. [Spoerke, Boal, Bachand et al. (2013); Bachand, Spoerke and Stevens (2015); Lubbe, Wezenberg and Feringa (2017)]. Therefore, understanding the fundamental mechanisms of different MT functions has triggered a lot of interests in both the experimental and theoretical manners. However, a lack of quantitative understanding in the energetic mechanics of both $\alpha\beta$ tubulin dimers and protofilament hinders advances in designing and controlling self-assembled functional structures from MTs.

A variety of experimental techniques have been used to investigate the mechanical properties of MTs, for examples, optical tweezers [Kurachi, Hoshi and Tashiro (1995)], hydrodynamic flow [Dye, Fink and Williams (1993)], thermally induced vibrations [Gittes, Mickey, Nettleton et al. (1993)], buckling in vesicles [Elbaum, Fygenson and Libchaber (1996)], atomic force microscopy [Kis, Kasas and Babić (2002)], and indirect tensile tests with a stretch chamber system [Kabir, Inoue, Hamano et al. (2014)]. Although great experimental achievements were reported, the underlying mechanism of the mechanics of MTs in terms of $\alpha\beta$ tubulin dimers remains largely unexplored since the multi-protofilament structure causes it difficult to establish a direct relation between molecular tubulin characteristics and experimentally observed MT properties. Hence, computational and theoretical methods are emerging to establish such a link and unveil the fundamental mechanism in the mechanical properties of MTs. For instance, several coarse-grained models [VanBuren, Cassimeris and Odde (2005); Ji and Feng (2011); Ji and Feng (2011); Zakharov, Gudimchuk, Voevodin et al. (2015)], in which each tubulin is modeled as a point mass, were developed to mimic the self-assembly kinetics of MTs and thus explain the underlying mechanisms. Tolomeo et al. [Tolomeo and Holley (1997)] developed a theoretical model based on classical beam theory to capture the mechanical properties of both a perfectly bonded bundle of microtubules and a perfectly frictionless unbonded bundle. Using this model, the bending stiffness change of microtubule bundles were explained, which resulted from the loss of cross-linking. Kasas et al. [Kis, Kasas and Babić (2002)] modeled microtubules as classical Euler-Bernouli beams using the finite element method and analyzed corresponding oscillation frequencies. Even though extensive efforts into the development of various models for microtubules has been devoted in recent years, a mesoscale finite element model (FEM) and structural mechanics beam model (SMBM) that can link the molecule-level and information to the overall performance of microtubules is still missing.

MD simulations have been serving as a basis to glean the molecular information and pass it to a high-level model, i.e. coarse-grained model and/or continuum model. In this paper, we first offer a straightforward molecular simulation approach to obtain detailed

molecular level information, including mechanical interactions between and within $\alpha\beta$ -tubulin heterodimers and per-residue energetic analysis. Then we proposed a FEM and SMBM using information extracted from molecular dynamics simulations as input. The FEM and SMBM offer an alternative strategy to address the mechanical behavior of PF. These integrated computational techniques will be employed to investigate the mechanical behavior of the $\alpha\beta$ -tubulin and protofilament under load applied (tension, bending, and torsion). Its capability to capture the mechanical properties are tested and compared with each model and also compared with existing simulations and experimental data for the validation.

2 PF modelling

A microtubule configuration was generally like a cylindrical hollow tube made up of PFs gathered together in parallel to each other along the circumferential direction. Typically, a microtubule is composed of 8~13 PFs, and it usually has an inner diameter of 15.4 nm and an outer diameter of 25 nm [Mofrad and Kamm (2006)]. The length of MT can vary from tens of nanometers to hundreds of microns. In our study, PF was composed of 10 spherical tubulins with α -tubulin and β -tubulin forming a dimer. Each tubulin is made in 6 nm diameter.

2.1 Molecular dynamics model (MDM)

Schematic geometry of MDM is shown in the Fig. 1a. As shown in Fig. 1a, a microtubule is a tubular structure inside cells. Tubulin dimers on the other hand are composed of α - and β -tubulins and are the building blocks of microtubules. The three-dimensional structure of the tubulin dimer was obtained from the PDB file indexed "1tub" [Nogales, Wolf and Downing (1998)] from the RCSB protein data bank. It is worth noting that the description of topologies of guanosine diphosphate (GDP) and guanosine triphosphate (GTP) was extracted from the existing topologies of adenosine diphosphate (ADP) and adenosine triphosphate (ATP). To describe the interaction among atoms in $\alpha\beta$ -tubulin dimer, the CHARMM36 [Best, Zhu, Shim et al. (2012)] force field was adopted. Our MD simulations revealed two possible orientations of the dimer. One can be forced apart leading to an elongated orientation of the dimer, and the second can be forced by producing a flexural orientation of the dimer.

The form of the potential energy function is given as follows:

$$E = E_{bond} + E_{angle} + E_{dihedrals} + E_{impropers} + E_{Urey-Bradley} + E_{vdw} + E_{elec},$$

where the first five terms account for short-range bonding interactions while the last two terms are associated with long-range van der Waals and electrostatic interactions. The cutoff distance for van der Waals and electrostatic interactions was set to be 12 Å. All molecular dynamics simulations were performed using the Nanoscale Molecular Dynamics (NAMD) [Nelson, Humphrey, Gursoy et al. (1996)] package. The environmental temperature was set at 310 K and the time step was set at 2 femtosecond. First, the tubulin dimer was immersed into a spherical water droplet with a 6.4 nm radius. The tubulin dimer was placed into water, also called solvation, in order to more closely resemble the cellular environment. It is not necessary to make the shape of the water box

spherical. However, energy minimization and equilibration will deform the box into the most stable shape with minimal surface tension, and the most stable shape is a sphere. We need to admit that there are some other aspects of the cellular environment not reflected in our current study, such as pH, concentration of ions, and interactions with other matters inside cellular plasma. These factors do play a very important role in determining the mechanical properties of microtubules, which should be good topics for our future studies. Subsequently, a 10-picosecond equilibration was run to obtain a stable configuration. More detailed can be found in recently published paper [Liu, Pidaparti and Wang (2017)]. Next, steered molecular dynamics (SMD) simulations were performed to test the intra-dimer interaction strength. The procedure for conducting steered molecular dynamics can be briefly described as follows. The backbone atoms of α -tubulin were fixed while the backbone atoms of β -tubulin were attached to a SMD atom through a virtual spring as shown in Fig. 1a. During the simulations, the SMD atom moved at a constant speed and the distance between the SMD atom and the center of the backbone atoms varied, resulting in force changes inside the virtual spring between them. The resultant force was uniformly distributed to all the backbone atoms of β -tubulin, leading to movement of those atoms and thus movement of the entire β -tubulin. The applied forces by the virtual spring can be expressed as follows,

$$\vec{F} = -\vec{\nabla} U,$$

$$U = \frac{1}{2} k [vt - (\vec{r} - \vec{r}_0) \cdot \vec{n}]^2,$$

where F is the force vector applied on the virtual spring, U is the potential energy, k is the stiffness of the spring, v is the moving velocity of the spring, t is time, \vec{r} is the actual position of the SMD atom, \vec{r}_0 is the initial position of the SMD atom and \vec{n} is the pulling direction. The stiffness of the virtual spring was 4.86 N/m and the moving speed was set at 1 m/s. Simulation results are analyzed and visualized through a visual molecular dynamics (VMD) [Humphrey, Dalke and Schulten (1996)] package.

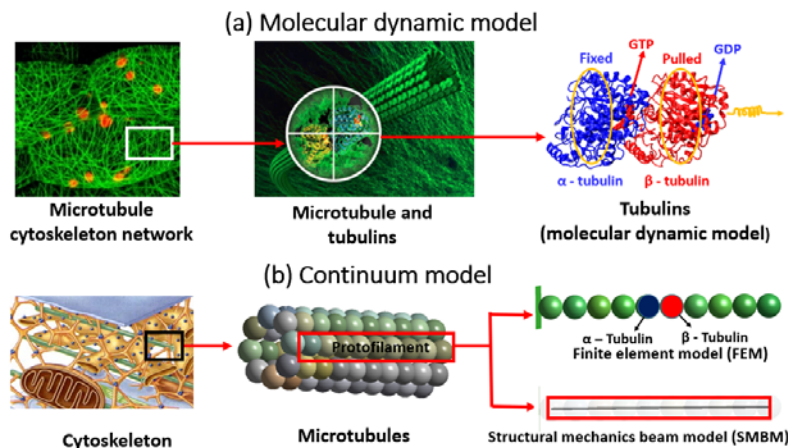


Figure 1: Multiscale structure of microtubule for (a) molecular dynamic and (b) finite element model. α and β tubulin in schematic view of both model are colored in blue and red, respectively

2.2 Finite element model (FEM)

The MD simulations can accurately describe the all-atom force fields and interactions between atoms/molecules. Hence, it is considered as a standard technique for the detailed studies of biomaterials. However, to date, the application of standard MD simulation is limited to relatively small protein complexes (typically comprising $\sim 10^5$ atoms). Therefore, further effort is demanded to develop a modelling technique that enables one to analyze the mechanical response of relative large biomaterials without any limitation on the size. To achieve this goal, and FEM in the spherical tubulin and in a protofilament is employed respectively. It was generated using ANSYS DesignModuler and each tubulin was connected with a spring at the contact region which represents MT protein stiffness.

2.2.1 Spring connection in FEM

Springs are useful in simulating filamentous network, enabling to accurately model intrinsically intricate geometries ubiquitous in cell biology studies [Kim, Hwang and Kamm (2009); Peter and Mofrad (2012)]. In addition to, spring connection captures higher level deflections of the PF, such as bending and axial deflections, using interaction potentials between tubulins that approximate the mechanical equation [Peter and Mofrad (2012)]. This formation can handle sufficient complexity with modest computational demand. Here, the MT protofilaments are represented by spherical shells (Fig. 1b), interacting linear spring element that represent elasticity, bending rigidity and torsional angle of MT protofilaments. Spring coefficients (stiffness), denoted by K_e , K_b , and K_t , stand for the tension, bending and torsion of PF, respectively. These spring constants are related to material properties of the PF in the equations:

$$K_e = E \cdot A / L \quad (1)$$

$$K_b = E \cdot I / L \quad (2)$$

$$K_t = G \cdot J / L \quad (3)$$

where E is the Young's modulus of the PF, A is the cross-sectional area of the PF, I is moment of inertia, G is shear modulus, J is polar inertia, and L is length of PF.

2.2.2 Structural mechanics (SM) beam model

The material properties of a structural beam are equivalent with the bond between the tubulin in PF, and it is extracted from MD simulation. SMBM of the PF is depicted in Fig. 1b. The theory of structural mechanics indicates that the deformation of constitutive beam is entirely controlled by three stiffness parameters, such as the extensional stiffness $E \cdot A$, flexural stiffness $E \cdot I$, torsional stiffness $G \cdot J$, where E is Young's modulus, A is cross-sectional area, I is moment of inertia, G is shear modulus and J is polar inertia of the equivalent beam.

Assuming the bond between two neighboring tubulin monomers as an equivalent structural beam with a circular cross section, and PF can be treated as a space frame as shown in Fig. 1b. The mechanical behavior of such a space frame can be readily simulated by the computational technique of structural mechanics. Following the theory of structural mechanics, three parameters, the tensile resistance $E \cdot A$, the flexural rigidity $E \cdot I$, and the torsional stiffness, $G \cdot J$, need to be determined for the structural analysis.

Each deformation under tension, bending and torsion for FEM and SMBM is indicated in Fig. 2.

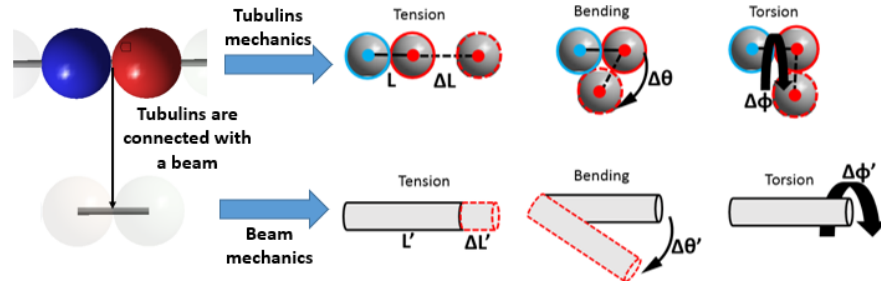


Figure 2: Deformation representation of FEM and SMBM

In the present SMBM of an PF, the aforementioned stretching, bending and torsion of the monomer bonds of FEM can be modelled by the tension, bending and torsion of the corresponding beams that construct the frame structure shown in Fig. 2. The total potential energy in the frame structure of an MT then reads

$$U = \sum U_A + \sum U_M + \sum U_T$$

where U_A , U_M and U_T are the strain energies of a beam due to tension, bending and torsion, respectively. With the known values of $E \cdot A$, $E \cdot I$ and $G \cdot J$, one can obtain the nodal displacements of the equivalent frame structures of PF following the standard solution procedure of the stiffness matrix method as detailed [Weaver and Gere (2012)].

We used ANSYS Workbench mechanical 16.0 to simulate our 3D FEM and SMBM. The chosen values of the parameters have been employed from our MD simulation and previous reports and it is indicated in Tab. 1. The material properties of the beam adopted in our study are obtained from the results in the previous study [Deriu, Enemark, Soncini et al. (2007); Peter and Mofrad (2012)]. According to a previous MD study, the stiffness of an individual α tubulin is around 11 N/m while that of a β tubulin is around 15.6 N/m [Deriu, Enemark, Soncini et al. (2007)]. The shear modulus of the spherical shell is set to be 400 MPa according to a recent study [Zeiger and Layton (2008)]. In our model, α tubulins are not differentiated from β tubulins due to their structural similarity and their mechanical performance. All simulations were performed using the software ANSYS 16.0 Mechanical package. We used ANSYS workbench to develop our 3D finite element model and analyzed it under different load types (tension, bending and torsion). The computational model adopted here consists of 104,000 nodes and 103,350 shell elements. Three different loading cases are tested for the protofilament as shown in Fig. 3: tension, bending, and torsion. For each loading case, the right end of the protofilament is fixed while the left end is applied with mechanical loading. SMBM simulations on the mechanical responses of MTs under tension, bending and torsion also were conducted in [Zhang and Wang (2014)].

Table 1: Parameters of material properties

Parameter		Value	Source
Tubulin radius (nm)		1.25	[Bates and Frenkel (2000)]
Tubulin surface area (nm ²)		1.57	Calculation
Tubulin volume (μm ³)		0.82	Calculation
Young's modulus (N/m ²)	FEM	1×10^9	[Howard (2001)]
	SMBM	0.8×10^9	[Zhang and Wang (2014)]
Shear modulus (N/m ²)		4×10^8	[Zeiger and Layton (2008)]
PF spring constant (nN/nm)	Axial	10.2-14.4	From our MD simulation
	Vertical	3.51-4.70	

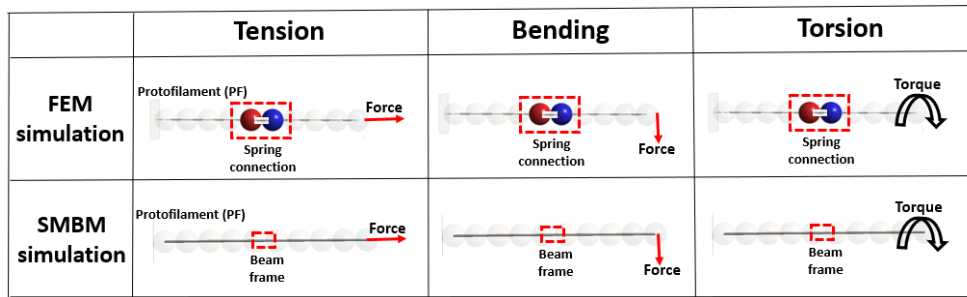


Figure 3: Representation of loading cases applied to PF of FEM and SMBM simulation: tension, bending and torsion

3 Results and discussion

3.1 MD simulation of $\alpha\beta$ -tubulin

In MD simulation, tension and bending tests were performed on the $\alpha\beta$ -tubulin dimer to analyze their interaction strength. Three independent runs were carried out for both tension and bending in order to obtain results with high accuracy. Relevant results obtained were used to calibrate the FEM and SM model. Due to the different initial velocity profiles, the force-displacement curves are different for different cases in atomic level MD simulation. Those differences come from thermal fluctuation. Fig. 4 shows the force-displacement responses in MD simulation. The force increases gradually until it reaches the peak under tension. The slope of the curve is not strictly constant, indicating the nonlinearity of the tubulins interaction. As we can see, three curves involved are close to each other and the tension stiffness calculated based on these curves to quantify the interactions between two tubulins ranges from 10.2-14.4 nN/nm. For bending, the force also is nonlinearly increasing until it reaches the peak, however the magnitude is smaller than under tension. After reaching the peak, the force starts to decay. In this situation, the α - and β -tubulins start to separate from each other. This finding shows good agreement with the results in a recent study [Alushin, Lander, Kellogg et al. (2014)] that indicates the interaction of inter-dimer or inter-protofilament. Resultant bending stiffness to

quantify the interactions between two tubulins ranges from 3.51-4.70 nN/nm. According to the coarse-grained MD simulations on MTs in Ji et al. [Ji and Feng (2011)], the values of stiffness are $kr=14$ nN/nm, $k\phi=3$ nN/nm, $kt=0.04$ nN·nm/rad² for $\alpha\beta$ interactions for tension, bending and torsion respectively.

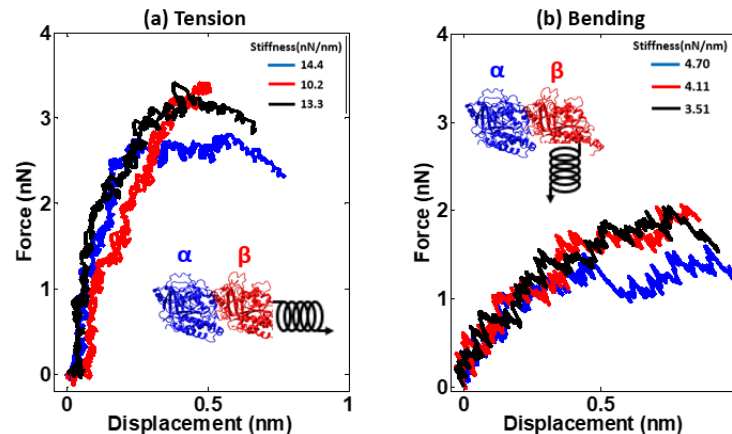


Figure 4: Force-displacement response under (a) tension and (b) bending between α - and β -tubulin in molecular dynamics (MD) simulation. Several different stiffness was employed

The peak tension stiffness between two tubulins is 14.4 nN/nm from our MD simulation, which is smaller than 44.7 nN/nm obtained in a recently published study [Deriu, Enemark, Soncini et al. (2007)]. It is important to note that in the recent published work, the calculation of the dimer stiffness did not take the deformation of β -tubulin into account, making the tension stiffness greater than that measured in our MD simulation. In our molecular dynamic simulation's setup, the α carbon atoms of α -tubulin were fixed while the α carbon atoms of β -tubulin were attached to the molecular dynamics atom through a virtual spring. Therefore, the deformation of individual tubulins are already included the resultant stiffness is a combination of the binding stiffness between two tubulins and intrinsic stiffness of individual tubulins. Another important quantity regarding mechanical responses is the rupture force, or the maximum force, approximately 3.32 nN.

3.2 FEM and SMBM simulation of $\alpha\beta$ -tubulin

In a computational simulation of FEM and SM, we analyzed the interaction between α - and β -tubulin in the middle of the protofilament. The tension, bending and stiffness values we used in this FEM and SM simulation are 12 nN/nm, 4 nN/nm respectively, which are the averaged value from the molecular dynamics simulation (Fig. 4). However, for the torsion, we employed torsional stiffness as 0.04 nN·nm/rad² in a previous report from Ji et al. [Ji and Feng (2011)]. Fig. 5 shows contour of displacement on a PF in three different loading cases. Under tension, the protofilament deforms on the axial axis accordingly with the displacement gradually increasing from the left end to the right end, which is reasonable. The maximum displacement is 20 nm. Under vertical loading, the protofilament experiences vertical deflection increasing from the left end to the right end and

the maximum displacement is around 80 nm. When torque is applied on the right end, the protofilament is twisted with displacement increasing from 0 on the left to 20 nm on the right. Note that the torsion displacement is converted from torsion angle by multiplying the diameter of the tubulin dimer. The finding in Fig. 5 is well agreed with Zhang et al. [Zhang and Wang (2014)]. Although the general trends of deformation could be recognized in the contour plot, the accurate deformation information is still ambiguous.

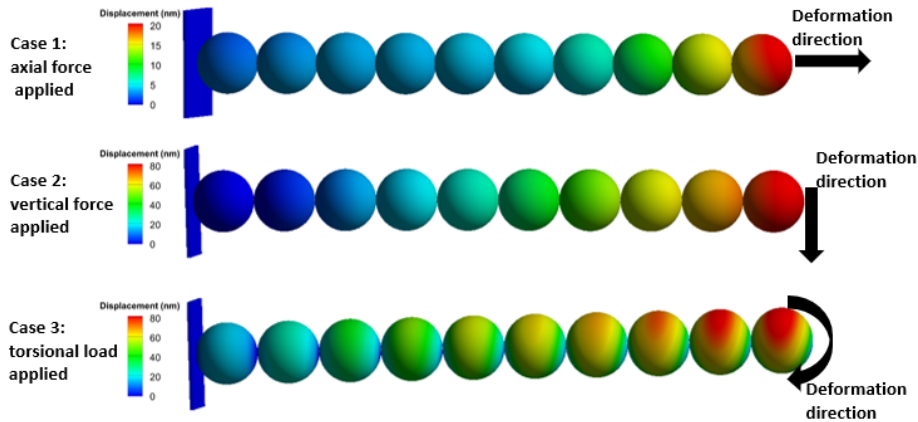


Figure 5: Contour of displacement for protofilament in microtubule

Fig. 6 displays the displacement of these contact regions between adjacent tubulins. As shown in Fig. 6, the displacement under tension increases slowly close to the left end and sharply close to the right end, indicating the intrinsic nonlinear elasticity of PF. However, under the bending, the transverse deflection increases linearly from contact region 1-9. The aspect ratio of this PF is a moderate 10 and thus the shear still plays a very important role in the deformation of the PF. Under torque, the displacement of the contact region in PF increases nonlinearly from the left end to the right end.

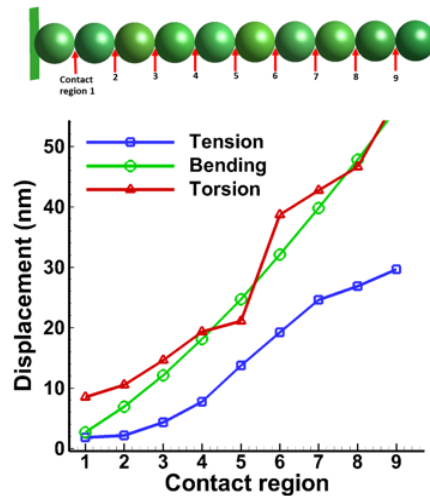


Figure 6: Displacement on the contact regions for PF under tension, bending and torsion

The comparison among MD, FEM, and SMBM for the force-displacement responses at middle tubulins under tension, bending and torsion shows in Fig. 7. From the comparison between the FEM, SM simulation and the MD simulation, the differences are marginal in Fig. 7. The middle tubulins are deformed with displacement gradually increasing. The slope of the curve indicates the nonlinearity of the tubulins interaction under tension and bending, however it displays quite linearity under torsion. The magnitude of the displacement for the bending is greater than under tension. The finding for FEM simulation of tubulins under bending is also consistent with the result of MD simulation of tubulins. The SMBM simulation result indicates the loadings (tension, bending and torsion) corresponding to each displacement is greater than MD and FEM simulation. FEM simulation result for all loading corresponding to each displacement is slightly greater than MD simulation. Relationship between torsional force and angle on middle tubulins is quite linear.

The results obtained are directly comparable to results from MT experiments [Kurachi, Hoshi and Tashiro (1995); Kis, Kasas and Babić (2002)]. In contrast, no direct experimental measurements on the dimer (tubulin) are available for comparison. Previously, experimental works have estimated the dimer's mechanical properties starting from the MT structure [Gittes, Mickey, Nettleton et al. (1993)]. Apart from the difficulties in separating the dimer's mechanical properties from the lateral and inter-dimer interactions, these simulations in our study can provide detailed knowledge about the individual dimer and their specific interactions. Also, our model has some limitations (ignoring velocity of tubulins and viscoelasticity of material). The single monomer measurements are done at a particular velocity [Deriu, Enemark, Soncini et al. (2007)]. However, tubulin structures are known to have viscoelastic properties, consequently the strain rate imposed can influence the obtained displacement results. Strain rates imposed in pulling/compression experiments of literatures on tubulins were in the order of 10^{-9} nm/ps [Lenne, Raae, Altmann et al. (2000)], while this influences the elastic constant values.

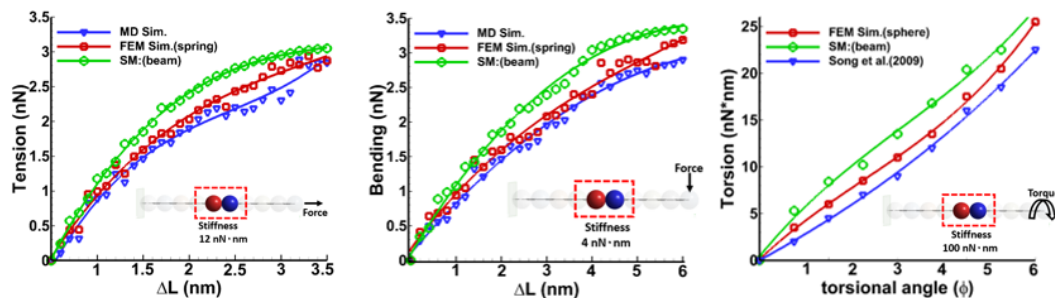


Figure 7: Force-displacement response under tension, bending and torsion between α - and β -tubulin in the middle of the protofilament by MD, FEM and SM simulation

Now in Fig. 8, the mechanical performance of PF under different loads (tension, bending, and torsion) are investigated for FEM and SMBM. Fig. 8 depicts the strain of the PF is showing that increases as stiffness increases for all types loading in FEM and SMBM. The response between stiffness and strain under all types load are showing nonlinearity, and the stiffness of SMBM under all types loads is higher than FEM. The magnitude of

stiffness for the tension is greater than bending. Previous study [Wells and Aksimentiev (2010)] introduced strains for a PF under applied force. In that study, the strain was calculated by fitting a PF to the xy coordinates of the centers-of-mass for each trajectory frame. In our study, the average strain on the PF for FEM and SMBM was collected by finite element method. The force-strain responses of the PF under different loads from the previous research [Wells and Aksimentiev (2010)] would be well compared to our simulation result. In that report, the force increases associated with the increase of strain and the strain exhibited an initial high resistance to deformation, to strains of ~ 0.2 . The change in resistance to deformation at ~ 0.2 may represent a transition from elastic to plastic deformation. By comparison, it can be easily recognized that the strain transition of curves for bending and torsional stiffness show at approximately 0.2, indicating that the current models (FEM and SMBM) can well capture the mechanical performance of PF.

The FEM simulation of a PF under tension allowed calculating mechanical characteristics. The Young modulus used in this study is 1 GPa in agreement with data reported in the literature. Up to date, all the experimental works in the past produced a wide range of values for mechanical characteristics of the microtubule (0.1-2.5 GPa) [Kurachi, Hoshi and Tashiro (1995); Kis, Kasas and Babić (2002)], and the most of these studies reported a Young modulus of 1-2 GPa. Spring elements representing in FEM for the single protofilament deformations and all monomer interactions were defined based on the elastic behavior obtained by MD. [Deriu, Enemark, Soncini et al. (2007)] reported the bending force-elongation curve for a 1 μm long PF elongated until 10% shows a linear behavior with slope 335 pN/nm. The Young modulus in that previous study was calculated assuming PF as a hollow cylinder with a cross section of 206.5 nm^2 based on force and displacement data at 10% of PF strain. Our results for bending and torsional stiffness are also linearly varying at 10% of PF strain.

It is evident that both force-displacement and stiffness-strain relationship shown in Figs 7-8 showed a similar trend, between present FEM and SMBM approaches. The difference may be attributed to using different tubulin properties as well as geometric models as input to the FEM and SMBM approaches. In our FEM, the tubulin stiffness properties obtained from molecular dynamics simulations were used whereas in SMBM approach, the stiffness corresponding to three different models of tubulin deformations were used. The tubulin stiffness properties used in our FEM are comparable to those reported in the literature [Gittes, Mickey, Nettleton et al. (1993); Howard (2001)]. Also, the differences between the stiffness obtained in our FEM and SMBM approaches are due to modeling and simulations of the actual protofilament (PF). For SMBM, the Young's modulus E rises and falls around a mean value 0.83 GPa with the maximum value around 0.85 GPa and minimum value around 0.8 GPa [Zhang and Wang (2014)]. Thus, the average Young's modulus of 0.83 GPa should be adequate in describing the Young's modulus for overall mechanical response of PF. In particular, it was found that the mean value of Young's modulus of 0.83 GPa predicted based on the SMBM for different PF agrees well with 0.8 GPa obtained in an experiment [Schaap, Carrasco, de Pablo et al. (2006)]. Our simulation result was well agreed with 0.8 GPa~0.9 GPa.

Experimental observations have shown that PFs frequently bend in living cells, with a mean curvature of about 0.4 rad/nm in fibroblast cells [Odde, Ma, Briggs et al. (1999)].

In general, PFs are responsible for mechanical rigidity of the cell. The bending deflection of SMBM for PF increases along the axis of the PF while there is no obvious variance in displacement in the transverse displacement. The bending of SMBM indicates the displacement of the right end versus vertical loadings, in which the deflection increases nonlinearly associated with the increase of vertical loadings. This behavior of PF can be explained by the Euler beam theory. There exist two possible physical origins, first is the effect of transverse shear deformation proposed for classical beams in the Timoshenko beam theory [Pampaloni, Lattanzi, Jonáš et al. (2006); Gao and Lei (2009)], and second is the nonlocal effect expected for nanoscale beams like PF [Wang, Li and Adhikari (2009)]. According to the Euler beam theory, the deflection on the right end can be described by the following formula: $\delta_{max} = \frac{Pl^3}{3EI}$, meaning that the displacement is proportional to the force applied.

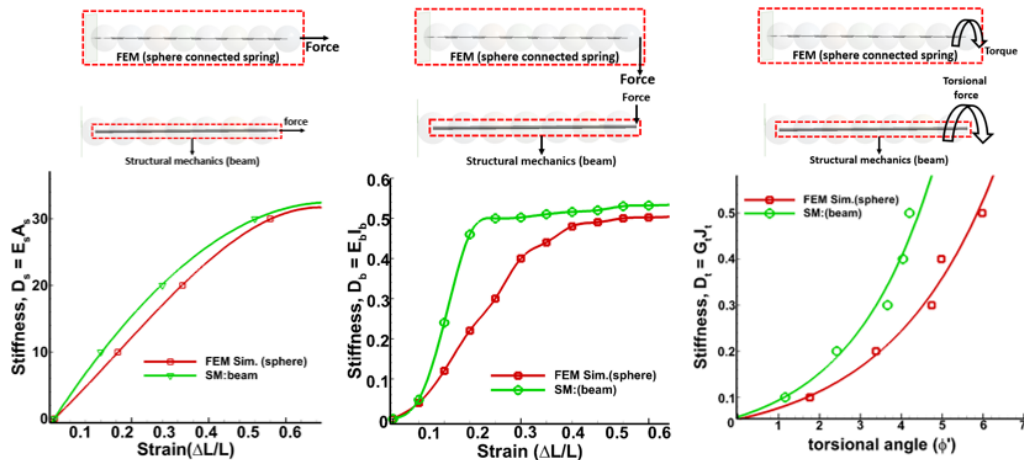


Figure 8: Comparison of stiffness-strain response under tension, bending and torsion for the PF by FEM and SM simulation

4 Conclusions

A FEM and SMBM for microtubule based on molecular level information has been developed, and its capability to capture mechanical properties has been displayed through simple loading cases (tension, bending and torsion) on PF. α and β tubulins, building blocks of PF, are modeled as spherical hollow shells with nonlinear elasticity which are connected by linear springs. The parameters involved in the model, such as stiffness of springs connecting adjacent tubulins, are derived from information extracted from molecular dynamics simulations. Tension, bending and torsion tests are performed on the PF. Results indicate good agreement among MD/FEM/SMBM simulation. In addition, the PF behaves non-linearly under loading cases. The stiffness-strain response can be attributed to the dominative role of shear deformation of FEM and SMBM. The deformation pattern can be well captured by the classical Euler beam theory and the flexural rigidity derived is in good agreement with those in the literature. The research findings here provide a reliable FEM and SMBM in simulating mechanical behaviors of PF, which

could be used to deepen our understanding of the underlying mechanism of statics and dynamics of microtubules.

Acknowledgements: The authors thank NSF for supporting this work through a grant CDS&E-1610812.

Disclosure statement: No potential conflict of interests was reported by the authors.

References

- Alberts, B.** (2017): *Molecular Biology of the Cell*. Garland Science.
- Alushin, G. M.; Lander, G. C.; Kellogg, E. H.; Zhang, R.; Baker, D. et al.** (2014): High-resolution microtubule structures reveal the structural transitions in $\alpha\beta$ -tubulin upon GTP hydrolysis. *Cell*, vol. 157, no. 5, pp. 1117-1129.
- Bachand, G. D.; Spoerke, E. D.; Stevens, M. J.** (2015): Microtubule-based nanomaterials: Exploiting nature's dynamic biopolymers. *Biotechnology and Bioengineering*, vol. 112, no. 6, pp. 1065-1073.
- Bates, M. A.; Frenkel, D.** (2000): Phase behavior of two-dimensional hard rod fluids. *Journal of Chemical Physics*, vol. 112, no. 22, pp. 10034-10041.
- Best, R. B.; Zhu, X.; Shim, J.; Lopes, P. E.; Mittal, J. et al.** (2012): Optimization of the additive CHARMM all-atom protein force field targeting improved sampling of the backbone ϕ , ψ and side-chain χ_1 and χ_2 dihedral angles. *Journal of chemical theory and computation*, vol. 8, no. 9, pp. 3257-3273.
- Deriu, M. A.; Enemark, S.; Soncini, M.; Montevecchi, F. M.; Redaelli, A.** (2007): Tubulin: from atomistic structure to supramolecular mechanical properties. *Journal of Materials Science*, vol. 42, no. 21, pp. 8864-8872.
- Dogterom, M.; Surrey, T.** (2013): Microtubule organization *in vitro*. *Current Opinion in Cell Biology*, vol. 25, no. 1, pp. 23-29.
- Dye, R. B.; Fink, S. P.; Williams, R. C.** (1993): Taxol-induced flexibility of microtubules and its reversal by MAP-2 and Tau. *Journal of Biological Chemistry*, vol. 268, no. 10, pp. 6847-6850.
- Elbaum, M.; Fygenson, D. K.; Libchaber, A.** (1996): Buckling microtubules in vesicles. *Physical Review Letters*, vol. 76, no. 21, pp. 4078.
- Gao, Y.; Lei, F. M.** (2009): Small scale effects on the mechanical behaviors of protein microtubules based on the nonlocal elasticity theory. *Biochemical and Biophysical Research Communications*, vol. 387, no. 3, pp. 467-471.
- Gittes, F.; Mickey, B.; Nettleton, J.; Howard, J.** (1993): Flexural rigidity of microtubules and actin filaments measured from thermal fluctuations in shape. *Journal of Cell Biology*, vol. 120, no. 4, pp. 923-934.
- Howard, J.** (2001): *Mechanics of Motor Proteins and the Cytoskeleton*. Sinauer Associates, Inc.
- Humphrey, W.; Dalke, A.; Schulten, K.** (1996): VMD: Visual molecular dynamics. *Journal of Molecular Graphics & Modelling*, vol. 14, no. 1, pp. 33-38.

- Ji, X. Y.; Feng, X. Q.** (2011a): Coarse-grained mechanochemical model for simulating the dynamic behavior of microtubules. *Physical Review E*, vol. 84, no. 3.
- Ji, X. Y.; Feng, X. Q.** (2011b): Mechanochemical modeling of dynamic microtubule growth involving sheet-to-tube transition. *Plos one*, vol. 6, no. 12.
- Kabir, A. M. R.; Inoue, D.; Hamano, Y.; Mayama, H.; Sada, K.** (2014): Biomolecular motor modulates mechanical property of microtubule. *Biomacromolecules*, vol. 15, no. 5, pp. 1797-1805.
- Kasas, S.; Cibert, C.; Kis, A.; Rios, P. L.; Riederer, B. et al.** (2004): Oscillation modes of microtubules. *Biology of the Cell*, vol. 96, no. 9, pp. 697-700.
- Kim, T.; Hwang, W.; Kamm, R.** (2009): Computational analysis of a cross-linked actin-like network. *Experimental Mechanics*, vol. 49, no. 1, pp. 91-104.
- Kis, A.; Kasas, S.; Babić, B.; Kulik, A.; Benoit, W. et al.** (2002): Nanomechanics of microtubules. *Physical Review Letters*, vol. 89, no. 24.
- Kurachi, M.; Hoshi, M.; Tashiro, H.** (1995): Buckling of a single microtubule by optical trapping forces: Direct measurement of microtubule rigidity. *Cytoskeleton*, vol. 30, no. 3, pp. 221-228.
- Lenne, P. F.; Raae, A.; Altmann, S.; Saraste, M.; Hörber, J.** (2000): States and transitions during forced unfolding of a single spectrin repeat. *FEBS Letters*, vol. 476, no. 3, pp. 124-128.
- Liu, N.; Pidaparti, R.; Wang, X.** (2017): Effect of amino acid mutations on intra-dimer tubulin-tubulin binding strength of microtubules. *Integrative Biology*, vol. 9, no. 12, pp. 925-933.
- Lubbe, A. S.; Wezenberg, S. J.; Feringa, B. L.** (2017): Artificial microtubules burst with energy. *Proceedings of the National Academy of Sciences*, vol. 114, no. 45, pp. 11804-11805.
- Mofrad, M. R.; Kamm, R. D.** (2006): *Cytoskeletal Mechanics: Models and Measurements in Cell Mechanics*. Cambridge University Press.
- Nelson, M. T.; Humphrey, W.; Gursoy, A.; Dalke, A.; Kalé, L. V. et al.** (1996): NAMD: A parallel, object-oriented molecular dynamics program. *International Journal of Supercomputer Applications and High Performance Computing*, vol. 10, no. 4, pp. 251-268.
- Nogales, E.; Wolf, S. G.; Downing, K. H.** (1998): Structure of the $\alpha\beta$ tubulin dimer by electron crystallography. *Nature*, vol. 391, no. 6663, pp. 199.
- Odde, D. J.; Ma, L.; Briggs, A. H.; DeMarco, A.; Kirschner, M. W.** (1999): Microtubule bending and breaking in living fibroblast cells. *Journal of Cell Science*, vol. 112, no. 19, pp. 3283-3288.
- Pampaloni, F.; Lattanzi, G.; Jonáš, A.; Surrey, T.; Frey, E. et al.** (2006): Thermal fluctuations of grafted microtubules provide evidence of a length-dependent persistence length. *Proceedings of the National Academy of Sciences*, vol. 103, no. 27, pp. 10248-10253.
- Peter, S. J.; Mofrad, M. R.** (2012): Computational modeling of axonal microtubule bundles under tension. *Biophysical Journal*, vol. 102, no. 4, pp. 749-757.

Schaap, I. A.; Carrasco, C.; de Pablo, P. J.; MacKintosh, F. C.; Schmidt, C. F. (2006): Elastic response, buckling, and instability of microtubules under radial indentation. *Biophysical Journal*, vol. 91, no. 4, pp. 1521-1531.

Spoerke, E. D.; Boal, A. K.; Bachand, G. D.; Bunker, B. C. (2013): Templated Nanocrystal Assembly on Biodynamic Artificial Microtubule Asters. *ACS Nano*, vol. 7, no. 3, pp. 2012-2019.

Tolomeo, J.; Holley, M. (1997): Mechanics of microtubule bundles in pillar cells from the inner ear. *Biophysical Journal*, vol. 73, no. 4, pp. 2241-2247.

Valdman, D.; Atzberger, P. J.; Yu, D.; Kuei, S.; Valentine, M. T. (2012): Spectral analysis methods for the robust measurement of the flexural rigidity of biopolymers. *Biophysical Journal*, vol. 102, no. 5, pp. 1144-1153.

VanBuren, V.; Cassimeris, L.; Odde, D. J. (2005): Mechanochemical Model of Microtubule Structure and Self-Assembly Kinetics. *Biophysical Journal*, vol. 89, no. 5, pp. 2911-2926.

Walczak, C. E.; Cai, S.; Khodjakov, A. (2010): Mechanisms of chromosome behaviour during mitosis. *Nature reviews Molecular Cell Biology*, vol. 11, no. 2, pp. 91-102.

Wang, C.; Li, C.; Adhikari, S. (2009): Dynamic behaviors of microtubules in cytosol. *Journal of Biomechanics*, vol. 42, no. 9, pp. 1270-1274.

Weaver, W.; Gere, J. M. (2012): *Matrix Analysis Framed Structures*. Springer Science & Business Media.

Wells, D. B.; Aksimentiev, A. (2010): Mechanical properties of a complete microtubule revealed through molecular dynamics simulation. *Biophysical Journal*, vol. 99, no. 2, pp. 629-637.

Zakharov, P.; Gudimchuk, N.; Voevodin, V.; Tikhonravov, A.; Ataulakhanov, F. I. et al. (2015): Molecular and mechanical causes of microtubule catastrophe and aging. *Biophysical Journal*, vol. 109, no. 12, pp. 2574-2591.

Zeiger, A.; Layton, B. E. (2008): Molecular modeling of the axial and circumferential elastic moduli of tubulin. *Biophysical Journal*, vol. 95, no. 8, pp. 3606-3618.

Zhang, J.; Wang, C. (2014): Molecular structural mechanics model for the mechanical properties of microtubules. *Biomechanics and Modeling in Mechanobiology*, vol. 13, no. 6, pp. 1175-1184.